2011 50th IEEE Conference on Decision and Control and
European Control Conference (CDC-ECC)
Orlando, FL, USA, December 12-15, 2011

Toward Estimating Concentration Fields in Biological Hydrogels Using Point Sensors

Justin P. Mattimore Richard E. Groff William Kolodzey

Abstract— **This paper is motivated by problems from biology involving estimation of concentration fields in a tissue sample using point measurements given by optical contactless biosensors. Due to biological constraints, the sensors may only be sparsely distributed and intermittently monitored. This paper proposes a nonbiological experimental platform, based on hydrogel and dye diffusion, for studying the problem of concentration field estimation using point sensors. A reduced order model for the diffusion system is derived using Karhunen-Loéve-Galerkin method and a discrete time Kalman filter is used to estimate the concentration field. The estimator is then applied to experimental data consisting of subsampled images from a diffusion process. Performance is evaluated by comparing the state estimates to the original images. Future work will use the experimental platform to study the effects of spatial distribution and timing of sensor measurements, to examine the effects of additional dynamics such as advection and reaction, and to perform online identification of process parameters.**

I. INTRODUCTION

Biological cells react to local concentrations of chemicals, such as oxygen, glucose, and various signaling proteins, within their microenvironment. Moreover, cells coordinate behavior with their neighbors by creating, passing, receiving, and acting on chemical signals. Intercellular signaling plays a critical role in tissue-level cellular behaviors, such as differentiation, angiogenesis, and tumorigenesis. Cells react to thousands of different intra- and inter-cellular signals and environmental factors; nevertheless, many tissue-level behaviors, such as planar polarity [1], are predominantly mediated by a relatively small number of signals and factors passed between cells. In order to study how behaviors are organized at the tissue level, it would be ideal to directly record the evolution of the concentration fields of the set of relevant signals. In this paper, the set of concentration fields will be referred to as the "state" of the biological system. This is much coarser than the full state of the system, which would necessarily include an intractable number of inter- and intra-cellular signals and environmental factors.

It is difficult to quantitatively measure concentration fields across the volume of a sample without interfering with the underlying biological processes. Optical contactless biosensors provide a minimally invasive method to measure local concentrations of a specific chemical. The metal chelate class of biosensors [11], [7], [9] generally take the form of small (less than a few micrometers diameter) polymer beads or spheres coated with a compound that fluoresces with an intensity related to the local concentration of a specific selected chemical. The beads often contain a second compound that fluoresces at an environment-independent level to serve as a reference. Beads can be used with traditional fluorescence microscopy or with confocal microscopy to measure pointwise concentrations in two or three dimensions, respectively. Optical contactless biosensors have been developed for oxygen, CO_2, pH, and various biomolecules [3], [8], [6]. A related class of optical contactless biosensors are based on liposomes [13], [12].

Biofabrication refers to a collection of tissue-engineering technologies, derived from rapid prototyping, for patterning cell co-cultures in two-dimensional or three-dimensional structures [4]. By arranging cells to mimic natural tissue, biofabrication may be used ultimately to create improved *in vitro* pharmaceutical test samples or even to fabricate replacement organs from a patient's own cells. More immediately, biofabrication offers an important tool for studying intercellular communication by enabling the creation of samples in which initial cell arrangement, and hence local intercellular communication, is finely controlled. Intriguingly, since biofabrication creates samples by printing successive layers of cells, optical contactless biosensors could be incorporated into the fabrication process, producing tissue samples that mimic natural tissue but also contain sensors designed for monitoring local concentration levels of one or more chemicals or environmental variables.

A number of constraints are associated with using optical contactless biosensors for studying intercellular communication. First, the sensors introduce additional materials and structure to the sample, which may alter the biological processes being studied. In consequence, the concentration field should be reconstructed using a minimal number of sensors. Second, the beads are effectively point sensors, measuring concentration locally. In order to reconstruct the concentration field directly, a large, dense set of sensors would be required. Third, the sensors must be illuminated with UV light in order to fluoresce. Unfortunately, frequent illumination alters cell behavior and ultimately causes cell death due to phototoxicity. Thus, measurements cannot be taken continuously and, in fact, should be taken as infrequently as possible.

Ultimately motivated by the problem of estimating concentration fields over time from intermittent measurements by point sensors in a biofabricated system, we present in this paper a nonbiological experimental platform for studying the problem in a simplified setting. Specifically, the exper-

This research was funded in part by NSF EFRI Grant #0736007.

J. Mattimore (justin.mattimore@gmail.com), R. Groff (regroff@clemson.edu), and W. Kolodzey are with the Department of Electrical and Computer Engineering, Clemson University.

imental platform consists of a thin section of hydrogel in which a dye is deposited and allowed to diffuse. Camera images are processed to provide a "true" estimate of the entire concentration field for the dye, while specific pixel values can be selected as point sensors. This allows direct comparison between the "true" concentration field and an estimate generated from measurements distributed in space and time. The simple diffusion process was chosen as a starting point in order to establish a baseline performance for the estimator, before considering additional complications from advection, reaction, and cell behavior.

Section II will present the theoretical background for forming a reduced-order model for the diffusion equation and a Kalman filter for estimation of the reduced state. Section III will present numerical experiments. Section IV will present the physical system and accompanying experiments. Finally, Section V presents conclusions and directions for future work.

II. Background

In the motivating biological problem, diffusion, advection and reaction would simultaneously affect the concentration field, but in the present work attention is limited to diffusion only in order to provide an initial validation of the test platform and methodology. The two-dimensional diffusion equation is given by

$$\begin{aligned} \frac{\partial u}{\partial t} &= D\nabla^2 u \\ &= D\left(\frac{\partial^2 u}{\partial x^2} + \frac{\partial^2 u}{\partial y^2}\right) \end{aligned} \tag{1}$$

where u is the concentration field describing mass concentration at a place and time and D is the diffusion coefficient, a real valued constant determining the rate of diffusion.

The diffusion PDE describes a continuum, and the state u is infinite dimensional. A finite dimensional approximation of the state must be formed in order to simulate or to formulate an estimator for the system. In the Galerkin method, the state of a continuum system is approximated as a linear combination of finite set of orthonormal basis functions

$$u(x,y,t) = \bar{u}(x,y) + \sum_{i=1}^{N} a_i(t)\phi_i(x,y) \tag{2}$$

where $\bar{u}$ is a time-invariant function, ϕ_i are a set of basis functions depending only on position, and $a_i(t)$ are a set of time-varying coefficients. In the case of the Karhunen-Loéve basis used below, $\bar{u}$ is the ensemble average of the observation data set. Galerkin's method projects the dynamics of the continuum system, in this case diffusion, in order to form new dynamics that describe the evolution of the coefficients in Eqn. 2 in order to optimally approximate the solution to the continuum system. The dynamics take the form

$$\begin{aligned} \dot{a} &= \Gamma a + b \qquad a \in \mathbb{R}^N \\ y &= Ca \qquad\quad y \in \mathbb{R}^P \end{aligned} \tag{3}$$

and

$$[\Gamma_{ij}] = \int_\Omega \phi_i(x,y)\nabla^2\phi_j(x,y)dxdy \tag{4}$$

$$[b_i] = \int_\Omega \nabla^2\bar{u}(x,y)\phi_i(x,y)dxdy \tag{5}$$

where Ω is the domain over which the PDE is to be solved. For diffusion, the dominant slow dynamic behavior of the system can be captured with just a few appropriately chosen basis functions [2].

In the following work, the Karhunen-Loéve (KL) empirical basis will be used with the Galerkin method, which together are known as the Karhunen-Loéve-Galerkin (KLG) method. The KL basis functions are principal modes of the system extracted from an ensemble of system simulations or observations. The KL basis is computed by subtracting the ensemble average from the observations and then using singular value decomposition to find the principal modes. A detailed discussion of the derivation of the KL basis functions, known as the method of snapshots, and the subsequent Galerkin projection will be ommitted due to length consideration. For a detailed discussion of the KLG method, see for example [5], [10]. The key points for the present work are that the KLG method provides a set of basis functions and corresponding dynamics that are tuned to the combination of continuum dynamics, boundary conditions, and initial condition that are present in the ensemble of simulations or observations.

While Galerkin's method provides Γ and b for Equation 3, the output equation is determined by the locations of the P point sensors in the system. The observation vector is

$$y = [y_1 \;\; y_2 \;\; \cdots \;\; y_P]^T, \tag{6}$$

where y_i is the observed sensor value at the corresponding point (x_i, y_i) in the domain. Thus, $C \in \mathbb{R}^{P\times N}$ is given by

$$C = \begin{bmatrix} \phi_1(x_1,y_1) & \phi_2(x_1,y_1) & \cdots & \phi_N(x_1,y_1) \\ \phi_1(x_2,y_2) & \phi_2(x_2,y_2) & \cdots & \phi_N(x_2,y_2) \\ \vdots & \vdots & \ddots & \vdots \\ \phi_1(x_P,y_P) & \phi_2(x_P,y_P) & \cdots & \phi_N(x_P,y_P) \end{bmatrix}. \tag{7}$$

The discrete time Kalman filter estimates the state of the system by weighting sensor measurements and predictions given by the system dynamic model. It is assumed the system is sampled at uniform temporal increments t_s and with negligible delay.

Integrating Eqn. 3, the dynamics in discrete time are

$$a(t+t_s) = Fa(t) + G$$

with

$$F = e^{\Gamma t_s}, \qquad G = \int_0^{t_s} e^{\Gamma(t_s-\tau)} b \; d\tau.$$

The reduced-order discrete-time Kalman filter is given by

Kalman Gain

$$K_t = Q_{t,t-1}C^T[CQ_{t,t-1}C^T + V_s]^{-1}$$

Reduced Order Model State

$$\hat{a}_{t,t} = \hat{a}_{t,t-1} + K_t[Y_t - C\hat{a}_{t,t-1}]$$

Approximate Continuum State State

$$u = \bar{u} + \sum_{i=1}^{N} a_i(t)\phi_i(x)$$

Covariance Matrix Update

$$Q_{t,t} = [I - K_t C_s]Q_{t,t-1}$$

Predicted Next Reduced Order Model State

$$\hat{a}_{t+1,t} = F\hat{a}_{t,t} + G$$

Predicted Next Covariance Matrix

$$Q_{t+1,t} = FQ_{t,t}F^T + V_y$$

The state of the reduced-order Kalman filter is initialized by finding a minimum norm fit of the basis functions to the sensor values at $t = 0$ using the Moore-Penrose pseudoinverse (denoted by †),

$$C^{\dagger}[y_1\ y_2\ ...\ y_M]^T = [a_1(t=0)\ a_2(t=0)\ ...\ a_N(t=0)]^T$$

The state covariance matrix for the estimate is initialized to the noise covariance, $Q = V_y$.

III. Numerical Experiments

The performance of the state estimator was first verified through a series of numerical simulations, since the experiment may introduce unmodeled dynamics, e.g. advection, which would complicate validation.

The two dimensional diffusion equation (2) was simulated for diffusion coefficient $D = 1$ over domain $\Omega = [0,1] \times [0,1]$. The initial and boundary conditions are given by

$$\text{IC} \qquad u(x,y,t=0) = 1 \qquad x,y \in [0.3, 0.7]$$

$$\text{BC} \qquad \begin{matrix} \frac{\partial u(x,0,t)}{\partial x} = \frac{\partial u(x,1,t)}{\partial x} = 0 \\ \frac{\partial u(0,y,t)}{\partial y} = \frac{\partial u(1,y,t)}{\partial y} = 0 \end{matrix} \qquad \begin{matrix} x,y \in [0,1] \\ t = [0,\infty) \end{matrix}$$

The "true" state of the system was obtained using a high order approximation using rectilinear discretization of the domain in increments of 0.01. The dynamics were simulated in Matlab using finite difference approximations with a numerical method of lines solver. Since the diffusion equation and imposed boundary conditions are homogeneous, the total mass in the system, i.e. the integral of concentration u over the domain, is preserved through time.

The relative error was used to assess estimator performance,

$$e(t) = \frac{\|u(t) - \hat{u}(t)\|}{\|u(t)\|} \tag{8}$$

where $u(t)$ is the true solution and $\hat{u}(t)$ is the approximate solution, and the norms are in the $\mathcal{L}^2$ sense,

$$\|u(t)\| = \left(\int_{\Omega} (u(t))^2 dA \right)^{\frac{1}{2}}. \tag{9}$$

The performance of two different classes of reduced oder model estimators was examined, one based on KL bases and one based on Fourier bases. The KL basis was chosen to be 4^{th} order, i.e. $N = 4$, since the principal values corresponding to these modes contained more than 99.4% of the sum of all the principal values. The Fourier basis was chosen to be 16^{th} order to achieve comparable performance. More modes are required since the Fourier basis is not tuned to the dynamics of the continuum system.

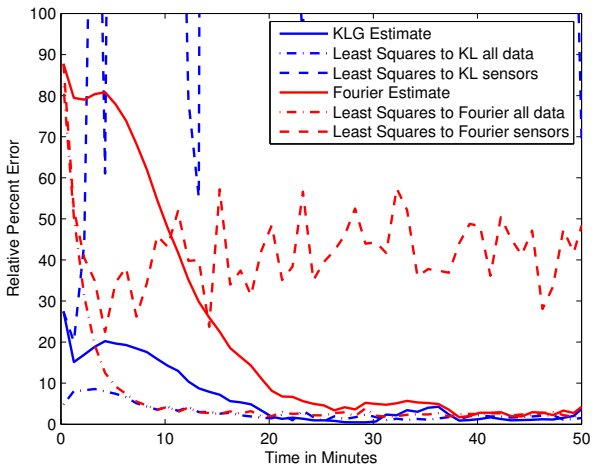

Fig. 1. Comparison of percent error of 4^{th} order Karhunen-Loéve-Galerkin (solid blue), 16^{th} order Fourier-Galerkin (dash-dotted red) and pseudoinverse fit to sensors measurements (dashed green) for numerical simulation of the 2D diffusion equation with additive white Gaussian noise.

The simulated data from the "true" model was corrupted with additive white Gaussian noise. The noisy data was sampled at 25 equally spaced locations in the domain and provided to the state estimators. The KL basis functions were computed from an ensemble of snapshots taken from a separate low order simulation of the expected initial condition.

Figure 1 presents the performance of the KLG- and Fourier-based reduced order model Kalman estimators. For comparison, the plot also includes two additional curves for each estimator: (*i*) the least squares projection of the full camera image onto the basis of the corresponding estimator, and (*ii*) the projection of the sparse sensor data onto the basis of the corresponding estimator. Note that (*i*) represents the smallest error attainable using the corresponding set of basis function, forming a strict lower bound for estimator performance, while (*ii*) represents the best estimate in terms of the corresponding basis given only sensor data from the current time step.

The KLG-based estimator model drives the error down the fastest, stays the lowest and reproduces the sharp initial condition the best. Both estimators provide superior performance compared to the least squares fits to available sensor data. The strong performance of the KLG reduced order model derives from the adaptation of the KL basis to the expected evolution of the system. Fig. 2 presents a numerical results illustrating the effects of initial condition mismatch. If the initial condition, and hence the snapshots used to construct the KL basis, are misleading or incorrect, then the performance of KLG degrades relative to the Fourier basis. In this set of simulations, the state estimator assumes the initial condition is in the center of the domain, while the

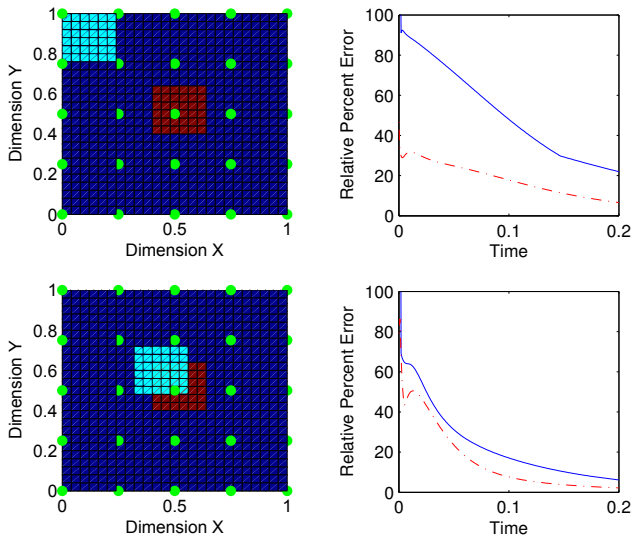

Fig. 2. [Right] Comparison of percent error of 4^{th} order Karhunen-Loéve-Galerkin (solid blue), 16^{th} order Fourier-Galerkin (dash-dotted red) for numerical simulation of noiseless 2D diffusion system with offset initial condition. [Left] The initial condition used for model generation is denoted in dark red while the actual initial condition tracked is denoted in teal.

initial condition of the true system is actually offset. The Fourier basis performed better in this case, since the KL basis was actually biased away from the best solution. In practical situations, the initial condition may only be poorly known.

IV. Physical Experiments

The state estimator was tested on experimental observations of a dye moving through a hydrogel.

A. Experimental Methods

A general test platform was developed for gathering experimental data for testing estimation of concentration fields. The platform could accommodate samples of varying size and boundary conditions. Samples were back lit via a Dolan-Jenner DC950 fiber optic light source diffused through frosted acrylic in order to produce a uniformly lit surface. The 13mm×13mm sample trays contained the gelatin samples and enforced a Neuman boundary conditions on the sample. An acrylic hood was placed over the samples to slow dehydration of the gelatin. Data was collected using a Lumenera Infinity microscope camera. A schematic representation of the test platform is depicted in figure 3.

Knox® brand flavorless gelatin was used as the hydrogel medium for studying diffusion. Gelatin, i.e. denatured collagen, serves as a low-cost biologically relevant hydrogel. The gelatin was mixed in a ratio of 3.55g gelatin to 236g water in order to tune the medium so that diffusion occurred over a couple hours while advection is limited or eliminated. The gelatin was held in an acrylic sample tray lined with paraffin to discourage dye advection in a layer under the gelatin. McCormick® blue food dye (water, propylene glycol, FD&C Blue 1, 0.1% propylparaben) was chosen as the dye for diffusion. The pigment is diluted to a 1.25% acqueous solution. The pigment source is injected into the gelatin at the beginning of the experiment using a syringe.

Images were taken every 15 seconds for 125 minutes using a Lumenera Infinity camera with microscope zoom lens. Each image was background subtracted from an initial image, converted to grayscale and cropped. The resulting grayscale values were directly interpreted as mass concentrations in these experiments. The ideal concentration profile would have highest concentration corresponding to gray value 255 and no concentration corresponding to 0. The image is resized into two data sets of 21 and 81 pixels square. Note that properties of the lighting, physical behavior of the dye, and camera sensor and settings may cause the relationship between mass concentration and grayscale value to be nonlinear. Similar effects are also present when taking measurements from optical contactless biosensors, especially saturation of the camera sensor and saturation of the dye. The results presented here could be further refined by taking these effects into consideration.

The diffusion coefficient of the aqueous solution of dye in gelatin was not initially known. The diffusion coefficient was fit to the experiment snapshots using a gradient descent approach. The first snapshot from the experimental data is used as the initial condition for the 2D diffusion equation and simulated with a coarse 21 element discretization on each axis. The algorithm runs simulations for differing diffusion coefficients until the integral of the relative error is minimized. The diffusion equation is then simulated at a fine 81 element discretization on each axis. The diffusion model fit using the gradient descent approach is simulated for the same time period as the physical experiment. The empirically fit diffusion coefficient was found to be $D = 119\mu\text{m}^2/\text{s}$ with standard deviation $18\mu\text{m}^2/\text{s}$ from a sample of 8 experimental runs.

The simulation snapshots are used to generate a Karhunen-Loéve basis with $N = 10$ modes and the corresponding dynamics are found using the Galerkin method. The reduced-order model is then used in a Kalman filter to estimate the state of the system from a sparse set of observations. Sparsely distributed point sensors are simulated by sampling only a few pixels from the images, chosen to be in the same relative locations as those in the numerical studies section. A state estimator based on a Fourier basis with $N = 16$ modes was also studied for comparison.

Estimator performance was evaluated in terms of relative error as defined in Eqn 8, where the true state u at time t is taken to be the corresponding camera image after background subtraction, cropping, and smoothing with an averaging filter to remove high spatial frequency camera noise.

B. Results and Discussion

Figure 4 presents the performance, in terms of relative error, of the KLG and Fourier state estimators for a typical experimental run. As with the numerical experiments, the plot also includes two additional curves for each estimator: (*i*) the least squares projection of the full camera image onto the basis of the corresponding estimator, and (*ii*) the

projection of the sparse sensor data onto the basis of the corresponding estimator.

The reduced-order KLG Kalman filter estimates the true state to within 20% relative error for most of the experiment. This relative error rate is considerably higher than seen in the numerical simulation, by almost a factor of 4. Nevertheless, the estimator performance is close to the performance of the least squares fit to the full camera image, indicating that much of the error arises because the experimental data is difficult to approximate for both the KL and Fourier basis families with current number of modes. In this case, increasing the number of modes would improve performance, whereas in the numerical simulations, increasing the number of modes would have had little effect.

The higher error of the state estimator for the first 20 minutes is most likely due to to an overestimate of the noise on the sensor data. This causes the estimator to place more trust in the current state estimate which in turn causes the estimate to slowly converge to the true state. The KLG estimator relative error is consistently several percent higher than the least squares fit of all camera data, indicating that better sensor placement improve the estimators ability to reconstruct the state.

Examining the time evolution of the simulated and experimental system calls attention to a problem with the system mass, i.e. the area integral of the concentration, illustrated in Figure 6. In the experimental system, mass appears to be increasing over time, whereas the simulated system has no source terms and Neumann boundary conditions, and therefore cannot accrue mass. The experimental system also has no source terms and Neumann boundary conditions, since (i) the only addition of mass (dye) occurred at the initial time, and (ii) the volume is finite so the mass may not flow out. This apparent increase in mass appears to be related to the way concentrations are interpreted from the camera. While concentration appears to be fairly linear over a wide range of concentrations, high concentrations get mapped to small range of low grayscale values, effectively saturating the sensor. The dye starts out highly concentrated and diffuses. The effect of sensor saturation is thus to make it appear that the system has a source term generating extra mass. This is an unmodeled dynamic in the current version of the system. Interestingly, similar saturation effects are present with optical contactless biosensors. When the local concentration of the target chemical is sufficiently high, then all the receptors in the sensors will be "filled" and fluorescing, and additional increases in local concentration will not change the level of fluorescence.

The apparent source term causes two problems. First, the diffusion coefficient is not known directly but fit to data through simulation, but fitting data with an apparent source term to a model without a source term will create systematic error. Second, the model which is formed using the Galerkin projection is composed of empirical orthogonal functions which are recovered from simulation of an homogeneous model. The Karhunen-Loéve-Galerkin reduced-order model can not reproduce dynamic behavior it has not seen before.

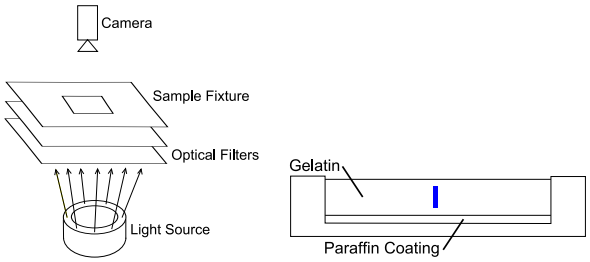

Fig. 3. [Left] A schematic of the test platform. A light source is diffused through filters producing a uniformly back lit fixture to hold the sample during observation. [Right] Cross section depicting the hydrophobic paraffin coating, gelatin and ideal ink injection in a sample tray.

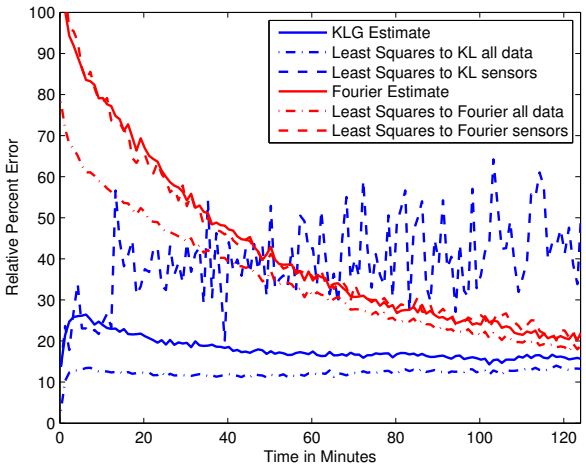

Fig. 4. Percent error plot of 10^{th} order Karhunen-Loéve-Galerkin and 16^{th} order Fourier-Galerkin state estimator of dye diffusing in gelatin. Least squares fit of each basis set using sensor data and all concentration data are plotted for comparison.

The diffusion coefficient could be characterized using an independent experiment, but improved methods of handling sensor saturation are still needed.

V. Conclusion and Future Work

This paper has demonstrated an experimental platform for studying the biologically motivated problem of estimating concentration fields from intermittent, pointwise sensor measurements. The use of a camera to measure dye diffusion gives a "true" measurement of the field against which to compare estimator performance. Estimators for the concentration field were constructed using a Kalman filter applied to Karhunen-Loéve-Garlerkin and Fourier reduced order models. The estimators performed reasonably well at reconstructing the full concentration field, though not as well as predicted by simulation. Saturation of the sensor measurements were a major source of error for the estimators. The present work demonstrates the feasibility of using reduced order model estimators with a small number of modes and sensors to estimate concentration fields in diffusion systems.

There are a number of directions in which to extend the present work in order to meet the demands fo the target application as well as to develop this system as a potential

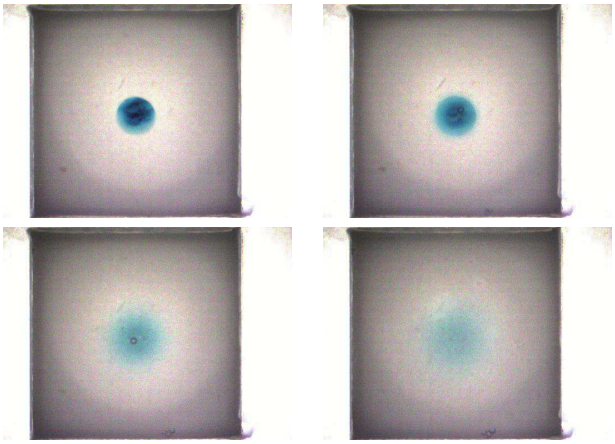

Fig. 5. Progression of blue dye diffusing in gelatin a 0, 10, 50, 90 minutes

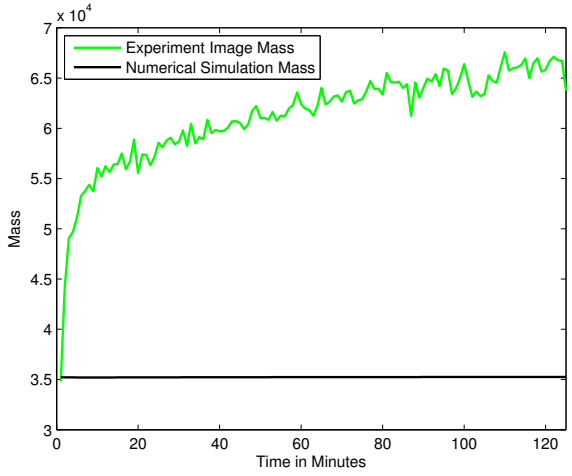

Fig. 6. Total mass, i.e. area integral of concentration, as measured by camera (green) and a numerical simulation using the first camera frame as the initial condition (black).

test bed for estimation theory: (*i*) To compensate for nonlinearities in the sensor when sensing high concentrations. This nonlinearity appears in the model system as well as when using optical contactless biosensors, and is thus of considerable practical importance; (*ii*) To analyze sensor placement to optimize the quality of information generated; (*iii*) To adjust time between sensor measurements in order to tradeoff the amount of information received from the measurement with the negative impact of the measurement. Cells suffer the more often they are exposed to UV light, so constant monitoring is not an option; (*iv*) To consider more complicated dynamics acting on the concentration field, such as posisition-dependent diffusion rates, advection and reaction; (*v*) To consider known-but-parametrically-uncertain dynamics and adapt the parameter online as the estimator runs, or alternatively to consider nonparametric models for the system dynamics.

REFERENCES

[1] K. Amonlirdviman, N. A. Khare, D. R. Tree, W. S. Chen, J. D. Axelrod, and C. J. Tomlin, "Mathematical modeling of planar cell polarity to understand domineering nonautonomy," *Science (New York, N.Y.)*, vol. 307, no. 5708, pp. 423–426, Jan 21 2005.

[2] J. Baker and P. Christofides, "Finite-dimensional approximation and control of non-linear parabolic pde systems," *Int. J. Control*, vol. 73, no. 5, pp. 439–456, 2000.

[3] S. Borisov, T. Mayr, and I. Klimant, "Poly(styrene-block-vinlypyrrolidone) beads as a versatile material for simple fabrication of opitcal nanosensors," *Analytical Chemistry*, vol. 80, pp. 573–582, 2008.

[4] T. Burg, C. A. P. Cass, R. Groff, M. Pepper, and K. J. L. Burg, "Building off-the-shelf tissue-engineered composites," *Philosophical Transactions of the Royal Society A-Mathematical Physical and Engineering Sciences*, vol. 368, no. 1917, pp. 1839–1862, APR 28 2010, pT: J.

[5] P. Holmes, J. Lumley, and G. Berkooz, *Turbulence, Coherent Structures, Dynamical Systems and Symmetry*. Cambridge, UK: Cambridge University, 1996.

[6] S. Im, G. Khalil, J. Callis, B. Ahn, M. Gouterman, and Y. Xia, "Synthesis of polystyrene beads loaded with dual lumiphors for self-referenced oxygen sensing," *Talanta*, vol. 67, pp. 492–497, 2005.

[7] I. Klimant and O. Wolfbeis, "Oxygen-sensitive luminescent materials based on silicone-soluble ruthenium diimine complexes," *Analytical Chemistry*, vol. 67, pp. 3160–3166, 1995.

[8] Y. Lee and R. Kopelman, "Optical nanoparticle sensors for quantative intracellular imaging," *Nanomedicine and Nanobiotechnology*, vol. 1, pp. 98–110, 2009.

[9] K. McNamara and Z. Rosenzweig, "Dye-encasulating liposomes as fluorescence-based oxygen nanosensors," *Analytical Chemistry*, vol. 70, pp. 4853–4859, 1998.

[10] A. Newman, "Model reduction via the karhunen-loéve expansion part i: An exposition," Technical Report T.R. 96-32, University of Maryland, College Park, MD., 1996.

[11] D. Papkovsky, T. O'Riordan, and A. Soini, "Phosphorescent porphyrin probes in biosensors and senstive bioassays," *Biochemical Society Transactions*, vol. 28, no. 2, pp. 74–77, 2000.

[12] M. Reppy and B. Pindzola, "Biosensing with polydiacetylene materials: structures optical properties and applications," *Chemical Communications*, pp. 4317–4338, 2007.

[13] Z. Yuan and T. Hanks, "A reversible colorimetric and flourescent polydiacetylene vesicle sensor platform," *Polymer*, vol. 49, pp. 5023–5026, 2008.